A Neutral Atom Frequency Reference in the Deep Ultraviolet with FractionalUncertainty = 5.7x10-15

John J. Mcferran, Lin Yi, Sinda Mejri, Sylvain Di Manno, Wei Zhang, Jocelyne Guéna, Yann Le Coq, Sébastien Bize

Neutral Atom Frequency Reference in the Deep Ultraviolet with Fractional Uncertainty $= 5.7 \times 10^{-15}$

J. J. McFerran,* L. Yi,† S. Mejri, S. Di Manno, W. Zhang, J. Guéna, Y. Le Coq, and S. Bize‡

LNE-SYRTE, Observatoire de Paris, CNRS, UPMC, 61 Avenue de l'Observatoire, 75014, Paris, France

(Received 25 December 2011; published 4 May 2012)

We present an assessment of the $(6s^2)\ ^1S_0 \leftrightarrow (6s6p)^3P_0$ clock transition frequency in ^{199}Hg with an uncertainty reduction of nearly 3 orders of magnitude and demonstrate an atomic quality factor Q of $\sim 10^{14}$. The ^{199}Hg atoms are confined in a vertical lattice trap with light at the newly determined magic wavelength of 362.5697 ± 0.0011 nm and at a lattice depth of $20E_R$. The atoms are loaded from a single-stage magneto-optical trap with cooling light at 253.7 nm. The high Q factor is obtained with an 80 ms Rabi pulse at 265.6 nm. We find the frequency of the clock transition to be 1 128 575 290 808 162.0 ± 6.4(syst) ± 0.3(stat) Hz (i.e., with fractional uncertainty $= 5.7 \times 10^{-15}$). Neither an atom number nor second order Zeeman dependence has yet been detected. Only three laser wavelengths are used for the cooling, lattice trapping, probing, and detection.

DOI: 10.1103/PhysRevLett.108.183004 PACS numbers: 32.30.Jc, 32.10.Dk, 37.10.Jk, 42.62.Fi

The advance in the performance of atomic clocks over recent decades is an impressive accomplishment by the adherents of time and frequency research. The accuracy of microwave clocks has improved at a rate of ~10 per decade and now optical clocks are showing an improvement at a rate $>10^2$ per decade [1]. Optical clock technology is still relatively young; yet several atomic species have demonstrated line-center frequency uncertainties near or below 10^{-16} [2–6], with the potential of several more to follow [7–9]. This will enable further precision in tests probing physics frontiers in the low energy regime [3,10–12]. Here we report on the substantially improved performance of a comparatively new neutral atom clock, one based on lattice-confined ^{199}Hg, which has the potential to outperform existing state-of-the-art neutral atomic clocks [7].

Ion clocks have demonstrated formidable results with respect to line frequency uncertainties [3,5,13] and progress is expected to continue. A prime driver for neutral atom clocks is the significantly higher number of quantum absorbers used for the atom-probe interaction. This provides an additional measurement lever by reducing the integration time required for assessing various clock shifts. The tightly bound atoms in an optical lattice trap become heavily immune to Doppler and photon-recoil effects (Lamb-Dicke regime). In the process of constraining the atoms, one needs to shift the upper and lower clock state energies by equal amounts by maintaining the lattice light at the magic wavelength [14]. Like other alkaline-earth-metal-type elements, mercury has a doubly forbidden transition between the ground $(ns^2)\ ^1S_0$ and the excited $(nsnp)\ ^3P_0$ levels ($n = 6$ for Hg). Its natural linewidth is ~100 mHz. It has several favorable characteristics for its use as a primary frequency reference, the most significant being that its sensitivity to blackbody radiation (BBR) is more than an order of magnitude lower than that of Sr and Yb [7,15]. The uncertainty due to the BBR dominates the frequency uncertainty budgets of these two clocks [4,16] (recent work shows a reduced uncertainty for the BBR shift in Yb of 3×10^{-17} [17]). Furthermore, the absence of a high temperature oven for Hg helps to reduce the temperature variations in the vicinity of the trapped atoms, thus helping to reduce the BBR uncertainty further.

Initial clock transition spectral widths measured for ^{199}Hg were about 2 kHz due to the delocalization of atomic states across lattice sites [18,19]. Here we have increased the lattice depth to at least $20E_R$ (recoil energy $= \hbar^2 k_l^2/2m$, k_l is the wave number, m is the atomic mass), forming more tightly bound atoms. A series of light shift measurements, permitting an improved estimate of the magic wavelength, in combination with Zeeman shift measurements has led to narrowing of the measured clock transition to ~10 Hz. The corresponding quality factor is 10^{14}, which has only previously been obtained in a limited number of systems, e.g., [4,5,20–22]. Along with the above mentioned systematic shift measurements we have investigated the atom number dependence and carried out a 3 month trial of absolute frequency measurements.

The ^{199}Hg atoms are loaded into a 1D vertical optical lattice from a single-stage magneto-optical trap (MOT) that uses laser light at 253.7 nm for the cooling ($^1S_0 \leftrightarrow {}^3P_1$). The MOT and lattice trap are described in detail in [19]. Some modifications have been made to the lattice cavity, which we outline below. A scaled drawing of the apparatus is shown in Fig. 1(a). On the left-hand side resides the combined MOT chamber and optical lattice cavity. The ports in the horizontal and 45° directions provide access for the MOT beams (from beneath). On the right-hand side is the mercury source chamber, which includes a 2D MOT setup. The 2D MOT is not employed in the measurements described here, but its use is anticipated in the future. Several grams of mercury are maintained at about −40 °C using a dual Peltier stage. Between 50 and

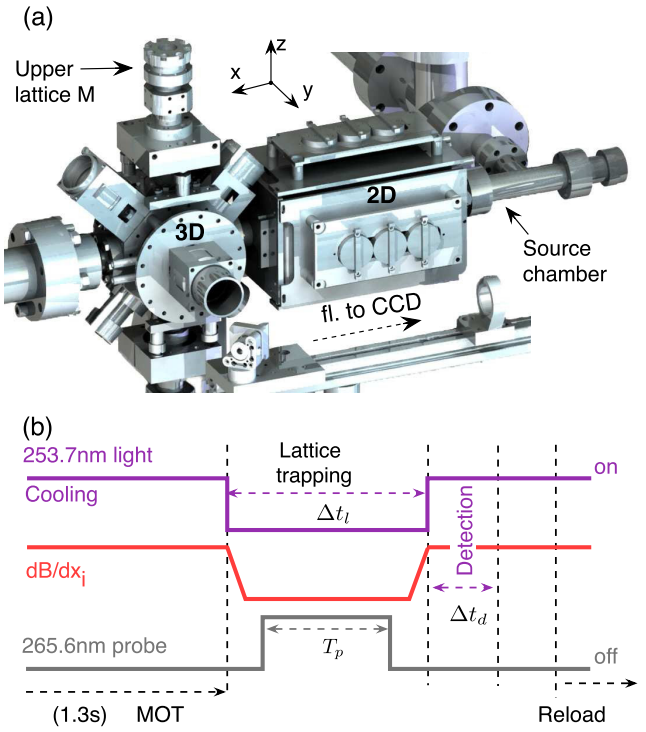

FIG. 1 (color online). a) Drawing of the vacuum system showing the 3D MOT (left side) and 2D MOT chambers. Also visible is the upper mirror of the optical lattice cavity above the 3D MOT chamber (note that fl. refers to fluorescence). (b) Timing sequence for the cooling light, probe light, and 3D MOT magnetic field gradient. The lattice light remains on continuously throughout the cycle. $\Delta t_l = 80$ ms and $T_p = 50$ ms for most measurements here; $\Delta t_d = 9$ ms.

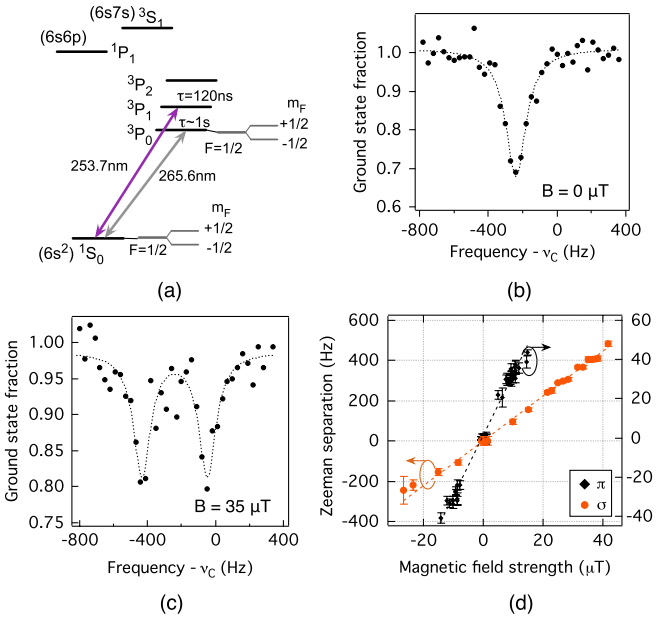

FIG. 2 (color online). (a) Partial level scheme for ^{199}Hg with hyperfine splitting of the ground and excited states. The 265.6 nm radiation is used to probe the $^1S_0 \leftrightarrow {}^3P_0$ clock transition ($\Gamma/2\pi \approx$ 100 mHz), while 253.7 nm radiation is used for cooling and detection. (b) A spectrum of the ^{199}Hg clock σ transition with $m_F = \pm 1/2 \rightarrow m_F = \pm 1/2$ Zeeman components overlapped. $\lambda_L = 362.573$ nm and FWHM = 140 Hz. ν_C is defined in the text. (c) Line profile of the ^{199}Hg σ transition showing the separated Zeeman components with FWHM = 120 Hz. (d) Frequency separation of the Zeeman components for the ultranarrow π and broadened σ transitions versus bias B field. The line gradients are 3.1 ± 0.2 Hz μT^{-1} and 11.1 ± 1.7 Hz μT^{-1}, respectively.

70 mW of 253.7 nm light is generated from a frequency quadrupling scheme for use in the 3D MOT (with the variation in power occurring over weeks or months).

The vertically orientated lattice cavity is comprised of two spherical mirrors, both with a radius of curvature of 250 mm. It has a finesse of 210 at 362 nm. The waist size (rad) is 120 μm where the lattice light overlaps the MOT cloud and produces a maximum lattice depth of $25E_R$ (or 9.2 μK). Light from a Ti:sapphire laser is frequency doubled in a LiB_3O_5 crystal based resonant cavity to produce light at or near the magic wavelength. This is coupled into the cavity from below and the transmitted light is used to side lock the Ti:sapphire laser to the lattice cavity (to maintain constant intensity). In our previous lattice cavity design there was a 45° reflector that formed an L-shaped cavity to lift polarization degeneracy [19]. This optic was found to degrade rather quickly under vacuum with the incidence of 362 nm light at high power and has been removed, enabling a deeper trap to be formed. The lattice light is linearly polarized in the x direction.

The $^1S_0 \leftrightarrow {}^3P_0$ clock transition lies at 265.6 nm, so as in the case of the 253.7 nm light generation, two frequency doubling stages are employed [see Fig. 2(a) for the relevant electronic transitions]. The infrared light at 1063 nm is sourced from a distributed feedback semiconductor laser, injection locked with light from a fiber laser tightly locked to an ultrastable optical cavity [23]. About 1 mW of 265.6 nm light is produced by the frequency quadrupling scheme. For rapid switching of the 265.6 nm probe light we employ an AOM, which positively shifts the frequency of the light by 180 MHz. An additional AOM, which is used to suppress noise in the fiber link between the ultrastable laser and the main Hg apparatus, is also used to tune the clock probe frequency (further details in [19]). Despite the drift rate of the ultrastable laser remaining below $+30$ mHz s^{-1} over the last five months, we still find it helpful to include a drift cancellation scheme to keep track of the clock transition. This is performed using a direct digital synthesizer that steers the frequency of the AOM in the 1063 nm path.

The profile of the clock transition is made via the detection of atoms in the ground state only and with the timing sequence shown in Fig. 1(b). A broad scan of the transition spectrum is shown in Fig. 2(b), where the magnetic bias field is made small enough that the $(^1S_0)m_F = \pm 1/2 \leftrightarrow (^3P_0)$ $m_F = \pm 1/2$ Zeeman components overlap one another. The frequency is offset by the value reported

in [24] for the ^{199}Hg transition frequency, i.e., $\nu_c = 1\,128\,575\,290\,808\,400$ Hz (and is applied to most of the plots below). We applied 1.5 μW of 265.6 nm light with a e^{-2} beam radius of 310 μm (intensity = 10 W m^{-2}). The full-width half-maximum (FWHM) is 140 Hz and the contrast ~32%. We show below that a much narrower transition lies at the center of this spectrum. The breadth of this line may be an indication that the transverse confinement of the atoms should be improved. When applying a dc B field, it separates into two Zeeman components [Fig. 2(c)] with slightly lower contrast and FWHM equal to 120 Hz. The Zeeman line separation versus the bias field strength is displayed in Fig. 2(d) (circles) exhibiting a slope of 11 Hz μT^{-1}. Since the 265.6 nm probe light copropagates with the lattice light, its polarization lies orthogonal to the axial direction of the lattice (i.e., in the horizontal plane). The bias B field is applied in the x direction, which is seen in Fig. 1(a). The probe light polarization was confirmed to be mostly linear, but shares a component in both x and y directions, allowing the possibility for both π and σ transitions. The 11 Hz μT^{-1} dependence corresponds closely to that expected for σ transitions [25]. Ideally the probe light polarization should be in the x direction, but in the present experiment the ultranarrow clock line strength (below) is optimized when the polarization has shared x and y components. The reason for this is still a matter for investigation. From the Zeeman dependence we conclude that the ~150 Hz wide feature is a broadened σ transition.

Information about the confinement of the atoms in the lattice trap is garnered by examining the sideband spectra of the Lamb-Dicke spectrum. Although not shown here, when we curve fit to the blue sideband using the approach outlined in [26,27] with the only free parameters being the lattice depth and the temperature in the radial direction, we find $U_0 = 18E_R$ (or 6.5 μK) and $T_r = 7$ μK, with associated axial and radial frequencies of 64 kHz and 43 Hz, respectively. We estimate the temperature of the atoms in the axial direction based on the ratio of the blue and red sidebands to be ~4 μK (with $P_n/P_{n+1} \sim 2.4$).

With the lattice light set at the magic wavelength (discussion below) and a higher resolution scan made across the center of the unsplit σ transition, we find a much narrower spectral line. Figures 3(a) and 3(b) show spectra obtained with $T_p = 50$ and 80 ms probe pulse durations taken with approximately 1 and 0.5 μW of 265.6 nm probe light, respectively. The solid lines are the modeled Rabi spectra with $\Omega.T_p \sim 1.4\pi$ rad for both. In Fig. 3(a) $\Omega.T_p$ was chosen in an attempt to match to the sidebands observed. While the width of the theoretical trace matches the data, the frequency of the sidebands in general does not, as seen in Fig. 3(b). From a measurement of the probe intensity we estimate the Rabi angle to be $\Omega.T_p \sim 4.5\pi$ rad. Despite this, we suspect that the sidebands are of a technical origin and are not due to an overdriven Rabi pulse, since reducing the probe power does not decrease the size

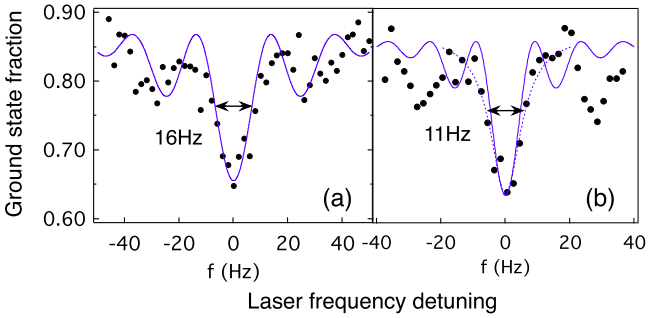

FIG. 3 (color online). Ground state fraction versus probe laser detuning frequency for (a) 50 and (b) 80 ms Rabi pulses. $\Omega T_p = 1.45\pi$ and 1.36π rad for the curve fits (solid lines), respectively. $B = 0$ and $\lambda_L \approx \lambda_m$ for (a) and (b).

of the sidebands. Nor does the frequency correspond to the radial trap frequency of ~45 Hz.

For most line-center measurements here we use a 50 ms probe. With an applied bias B field the narrow transition separates into two Zeeman components. The 1st order Zeeman dependence is seen in Fig. 2(d) with a slope of 3.1 ± 0.2 Hz μT^{-1}. The ratio of the B-field dependencies for the broadened σ transition versus the narrow π transition is ~3.6, which is close to the σ/π ratio of 3.3 that one expects when calculated from the difference in the Landé g factors of the ground and excited states [25].

For assessments of the ac Stark shift, the center frequency of the clock transition is measured at a series of lattice (vacuum) wavelengths and lattice depths. The results are summarized in Fig. 4(a). The main graph shows data taken with the 10–15 Hz wide spectral lines, while the inset shows lower resolution data obtained with the broader σ transition. From these data we determine the magic frequency to be 826.8546 ± 0.0024 THz ($\lambda_m = 362.5697 \pm 0.0011$ nm). The uncertainty also incorporates the accuracy of the wave meter used for the measurements. From the line fit we find that the strength of the light shift is $(-5.1 \pm 0.9) \times 10^{-17} E_R^{-1}$ GHz^{-1}.

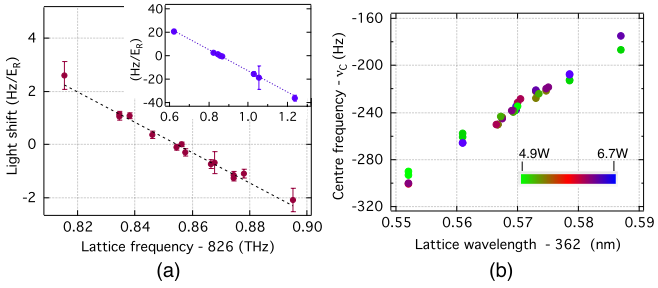

FIG. 4 (color online). (a) Differential light shift versus lattice frequency for the ^{199}Hg clock transition. The inset shows measurements made over a larger frequency range. The Stark-shift free frequency (wavelength) is 826.8546 ± 0.0024 THz (362.5697 ± 0.0011 nm) and the slope is -57 mHzE_R^{-1} GHz^{-1}. (b) Clock transition frequency versus lattice wavelength with changes of lattice power. (1W implies $3.5E_R$ for the trap depth.)

TABLE I. Corrections and uncertainties for the ^{199}Hg clock transition.

Effect	Correction (Hz)	Uncertainty (Hz)
Blackbody radiation	−0.17	0.2
1st order Zeeman	0	0.5
2nd order Zeeman	0	1.6
Scalar light shift (lattice)	0	5.9
Probe light	0.02	0.3
Atom number density	0.4	1.9
Total	0.2	6.4

Another representation of the light shift is shown in Fig. 4(b). Here the line-center frequency is plotted as a function of the lattice wavelength while some variation was applied to the lattice depth as indicated by the color scale. It shows directly the sensitivity of the clock transition frequency to the lattice wavelength. The small variation in the center frequency near 362.570 nm is consistent with the above magic wavelength determination. Here the strength of the light shift is $\sim -6 \times 10^{-17} E_R^{-1}$ GHz^{-1}.

A preliminary assessment of other systematic shifts affecting the ^{199}Hg clock transition has been conducted and is summarized in Table I. For a temperature uncertainty of 2 K of the chamber surrounding the atoms, and a 100% uncertainty for the calculated BBR coefficient [7], the shift at 290 K is -0.17 ± 0.20 Hz. A measurement of line-center frequency versus Zeeman component separation showed no variation within a statistical uncertainty of 1.6 Hz. This is expected since the predicted 2nd order Zeeman dependence is 2.16×10^{-9} T^{-2} (e.g., $B = 10$ μT produces a shift of 0.24 mHz) [7].

The frequency dependence on atom number has been tested by two means: (i) by varying the loading time of the MOT and (ii) by varying the level of 253.7 nm light used for cooling. Both methods change the number of atoms loaded into the lattice trap (and also the density since the size of the MOT cloud changes by less than 5% for the range considered here). The nominal atom number is $N_0 = 2.5 \times 10^3$ (close to the maximum that we achieve). Figure 5(a) shows the line-center frequency, ν_{Hg}, versus the relative atom number (N/N_0) obtained by varying the MOT loading time from 0.8 to 2.5 s. Figure 5(b) shows ν_{Hg} for a range of cooling light intensities with a slope equal to -0.11 ± 0.08 Hz per unit s_0 ($s_0 = I/I_0$, where $I_0 = 102$ W m^{-2}). The two results suggest a nonsignificant density shift at the present resolution. For daily assessments of line-center frequency (described below) there are between 10 and 30 spectra recorded. From a plot of center frequency versus relative atom number we determine the frequency shift at N_0, which we show in Fig. 5(c) for each measurement day where there was sufficient variation in N/N_0. From the weighted mean the frequency shift is constrained to 0.26 ± 1.9 Hz, consistent with the previous two results. Note, the number of atoms per site is of order 1 and the peak atomic density in the lattice is $\sim 3 \times 10^8$ cm^{-3}.

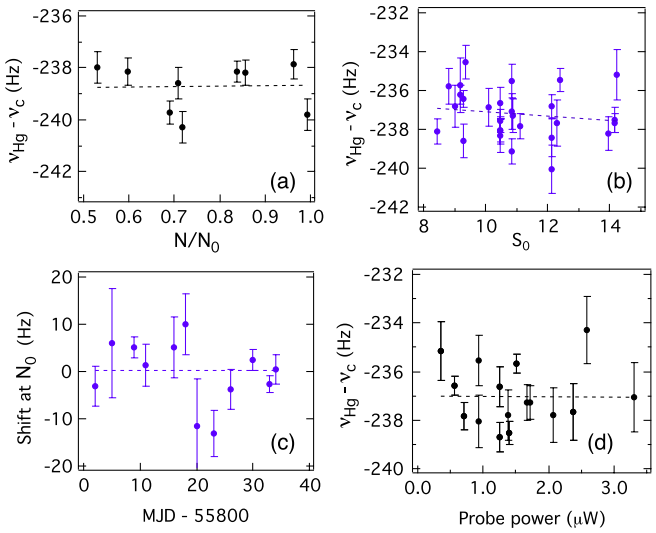

FIG. 5 (color online). Line-center frequency versus (a) relative atom number, where $N_0 = 2.5 \times 10^3$ and (b) MOT cooling light intensity, s_0. (c) Frequency shift at N_0 versus measurement day. (d) Line-center frequency versus probe power.

An ac Stark shift may also arise due to the probe light. In Fig. 5(d) we show the clock transition frequency versus the probe power. At our nominal power level of 1 μW the shift lies within the uncertainty of the measurement. We also calculate that the probe light shift is in the 1–10 mHz range. Hyperpolarizability shifts due to the lattice light are omitted from the table as they are expected to be at least an order of magnitude smaller.

Frequency comb accuracy has been verified by comparing measurements from two frequency combs (a Ti:sapphire comb and a Er:fiber based comb), which are steered by a low noise H-maser reference. The two combs show agreement to below 0.01 Hz. The H-maser reference is continually compared to the LNE-SYRTE frequency standard, which has a relative uncertainty of 2.7×10^{-16} [28]. An

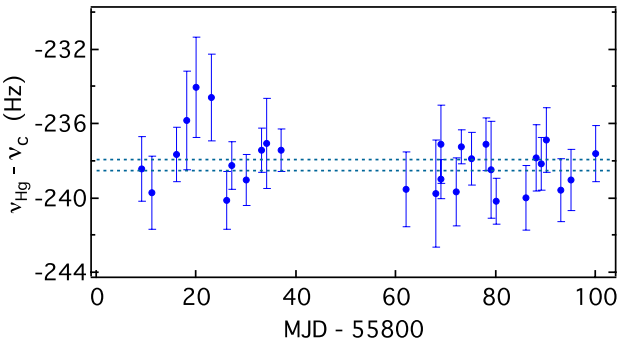

FIG. 6 (color online). Clock transition frequency measured over a three month period with respect to the SYRTE primary frequency standard for $\lambda_m = 362.5697$ nm. The weighted mean is $\nu_c - 238.2 \pm 0.3$ Hz. $\nu_c = 1\,128\,575\,290\,808\,400$ Hz.

example of the reproducibility of the clock transition frequency is shown in Fig. 6, where measurements have been made over a period of three months. Each point is the mean line-center frequency produced from between 10 and 30 spectra recorded on each day represented. The measurements were mostly performed with the two (π transition) Zeeman components overlapped due to the low S/N in the present experiment. The variations in frequency reduce after modified Julian day = 55 825 when we began controlling the lattice light frequency to within 300 MHz. The uncertainty of the weighted mean of this series is 0.3 Hz ($\sigma/\nu_{\mathrm{Hg}} = 2.5 \times 10^{-16}$). Accounting for the systematic shifts (Table I) we evaluate the $^{199}\mathrm{Hg}\,^1S_0 \leftrightarrow {}^3P_0$ transition frequency to be $1\,128\,575\,290\,808\,162.0 \pm 6.4(\mathrm{syst}) \pm 0.3(\mathrm{stat})$ Hz, where the combined fractional uncertainty is 5.7×10^{-15}.

This work establishes the potential of ^{199}Hg as a high-accuracy clock. There remain various means for further gains in accuracy; e.g., the S/N of the clock signal should improve as techniques for sideband cooling, transverse cooling, and atom number normalization are implemented, along with lattice trap depth enhancement. One also expects that a reliable means of producing >150 mW of 253.7 nm radiation will be found in which 2D-MOT loading should increase atom numbers tenfold [25].

The authors thank the Systèmes de Référence Temps-Espace technical support, in particular, M. Lours and F. Cornu. We thank G. Santarelli for the use of lab equipment, and D. Magalhães and L. Nenadović for assistance. This work is partly funded by IFRAF and CNES.

*john.mcferran@obspm.fr
†Present address: Jet Propulsion Laboratory, California Institute of Technology, Pasadena, CA 91109, USA.
‡sebastien.bize@obspm.fr

[1] H. Margolis, Contemp. Phys. **51**, 37 (2010).
[2] A. Ludlow, T. Zelevinsky, G. Campbell, S. Blatt, M. Boyd, M. de Miranda, M. Martin, L. Thomsen, S. Foreman, J. Ye, H. Fortier, E. Stalnaker, S. Diddams, Y. Le Coq, Z. Barber, N. Poli, H. Lemke, K. Beck, and C. Oates, Science **319**, 1805 (2008).
[3] T. Rosenband, D. Hume, P. Schmidt, C. Chou, A. Brusch, L. Lorini, W. Oskay, R. Drullinger, T. Fortier, J. Stalnaker, S. Diddams, W. Swann, N. Newbury, W. Itano, D. Wineland, and J. Bergquist, Science **319**, 1808 (2008).
[4] N. D. Lemke, A. D. Ludlow, Z. W. Barber, T. M. Fortier, S. A. Diddams, Y. Jiang, S. R. Jefferts, T. P. Heavner, T. E. Parker, and C. W. Oates, Phys. Rev. Lett. **103**, 063001 (2009).
[5] N. Huntemann, M. Okhapkin, B. Lipphardt, S. Weyers, C. Tamm, and E. Peik , Phys. Rev. Lett. **108**, 090801 (2012).
[6] C. W. Chou, D. B. Hume, J. C. J. Koelemeij, D. J. Wineland, and T. Rosenband, Phys. Rev. Lett. **104**, 070802 (2010).
[7] H. Hachisu, K. Miyagishi, S. G. Porsev, A. Derevianko, V. D. Ovsiannikov, V. G. Pal'chikov, M. Takamoto, and H. Katori, Phys. Rev. Lett. **100**, 053001 (2008).
[8] P. Dubé, A. A. Madej, J. E. Bernard, L. Marmet, J.-S. Boulanger, and S. Cundy, Phys. Rev. Lett. **95**, 033001 (2005).
[9] M. Chwalla, J. Benhelm, K. Kim, G. Kirchmair, T. Monz, M. Riebe, P. Schindler, A. S. Villar, W. Hansel, C. F. Roos, R. Blatt, M. Abgrall, G. Santarelli, G. D. Rovera, and P. Laurent, Phys. Rev. Lett. **102**, 023002 (2009).
[10] S. Blatt, A. D. Ludlow, G. K. Campbell, J. W. Thomsen, T. Zelevinsky, M. M. Boyd, J. Ye, X. Baillard, M. Fouche, R. Le Targat, A. Brusch, P. Lemonde, M. Takamoto, F. L. Hong, H. Katori, and V. V. Flambaum, Phys. Rev. Lett. **100**, 140801 (2008).
[11] T. Fortier, N. Ashby, J. Bergquist, M. Delaney, S. Diddams, T. Heavner, L. Hollberg, W. Itano, S. Jefferts, K. Kim, F. Levi, L. Lorini, W. Oskay, T. Parker, J. Shirley, and J. Stalnaker, Phys. Rev. Lett. **98**, 070801 (2007).
[12] S. G. Karshenboim and E. Peik, Eur. Phys. J. Special Topics **163**, 1 (2008).
[13] C. W. Chou, D. B. Hume, T. Rosenband, and D. J. Wineland, Science **329**, 1630 (2010).
[14] H. Katori, M. Takamoto, V. G. Pal'chikov, and V. D. Ovsiannikov, Phys. Rev. Lett. **91**, 173005 (2003).
[15] S. G. Porsev and A. Derevianko, Phys. Rev. A **74**, 020502 (2006).
[16] M. Swallows, G. Campbell, A. Ludlow, M. Boyd, J. Thomsen, M. Martin, S. Blatt, T. Nicholson, and J. Ye, IEEE Trans. Ultrason. Ferroelectr. Freq. Control **57**, 574 (2010).
[17] J. A. Sherman, N. D. Lemke, N. Hinkley, M. Pizzocaro, R. W. Fox, A. D. Ludlow, and C. W. Oates, Phys. Rev. Lett. **108**, 153002 (2012).
[18] L. Yi, S. Mejri, J. J. McFerran, Y. Le Coq, and S. Bize, Phys. Rev. Lett. **106**, 073005 (2011).
[19] S. Mejri, J. J. McFerran, L. Yi, Y. Le Coq, and S. Bize, Phys. Rev. A **84**, 032507 (2011).
[20] R. Rafac, B. Young, J. Beall, W. Itano, D. Wineland, and J. Bergquist, Phys. Rev. Lett. **85**, 2462 (2000).
[21] M. M. Boyd, A. D. Ludlow, S. Blatt, S. M. Foreman, T. Ido, T. Zelevinsky, and J. Ye, Phys. Rev. Lett. **98**, 083002 (2007).
[22] C. W. Chou, D. B. Hume, M. J. Thorpe, D. J. Wineland, and T. Rosenband, Phys. Rev. Lett. **106**, 160801 (2011).
[23] S. T. Dawkins, R. Chicireanu, M. Petersen, J. Millo, D. V. Magalhaes, C. Mandache, Y. Le Coq, and S. Bize, Appl. Phys. B **99**, 41 (2009).
[24] M. Petersen, R. Chicireanu, S. T. Dawkins, D. V. Magalhaes, C. Mandache, Y. L. Coq, A. Clairon, and S. Bize, Phys. Rev. Lett. **101**, 183004 (2008).
[25] M. Petersen, Ph.D. thesis, L'Université Pierre et Marie Curie, 2009, http://tel.archives-ouvertes.fr/tel-00405200/fr/.
[26] R. Le Targat, Ph.D. thesis, Ecole Nationale Supérieure des Telecommunications, 2007, http://tel.archives-ouvertes.fr/tel-00170038/fr/.
[27] A. D. Ludlow, M. M. Boyd, T. Zelevinsky, S. M. Foreman, S. Blatt, M. Notcutt, T. Ido, and J. Ye, Phys. Rev. Lett. **96**, 033003 (2006).
[28] Bureau International des Poids et Mesures (BIPM) Circular T, No. 281, May 2011, ftp://ftp2.bipm.org/pub/tai/publication/cirt.281.